

Home Search Collections Journals About Contact us My IOPscience

Voltage-sensitive dye imaging reveals improved topographic activation of cortex in response to manipulation of thalamic microstimulation parameters

This article has been downloaded from IOPscience. Please scroll down to see the full text article.

2012 J. Neural Eng. 9 026008

(http://iopscience.iop.org/1741-2552/9/2/026008)

View the table of contents for this issue, or go to the journal homepage for more

Download details:

IP Address: 128.61.139.105

The article was downloaded on 07/03/2012 at 15:58

Please note that terms and conditions apply.

doi:10.1088/1741-2560/9/2/026008

J. Neural Eng. 9 (2012) 026008 (14pp)

Voltage-sensitive dye imaging reveals improved topographic activation of cortex in response to manipulation of thalamic microstimulation parameters

Qi Wang, Daniel C Millard, He J V Zheng and Garrett B Stanley

Department of Biomedical Engineering, Georgia Institute of Technology/Emory University, Atlanta, GA 30332, USA

E-mail: qi.wang@bme.gatech.edu and garrett.stanley@bme.gatech.edu

Received 3 October 2011 Accepted for publication 3 January 2012 Published 13 February 2012 Online at stacks.iop.org/JNE/9/026008

Abstract

Voltage-sensitive dye imaging was used to quantify in vivo, network level spatiotemporal cortical activation in response to electrical microstimulation of the thalamus in the rat vibrissa pathway. Thalamic microstimulation evoked a distinctly different cortical response than natural sensory stimulation, with response to microstimulation spreading over a larger area of cortex and being topographically misaligned with the cortical column to which the stimulated thalamic region projects. Electrical stimulation with cathode-leading asymmetric waveforms reduced this topographic misalignment while simultaneously increasing the spatial specificity of the cortical activation. Systematically increasing the asymmetry of the microstimulation pulses revealed a continuum between symmetric and asymmetric stimulation that gradually reduced the topographic bias. These data strongly support the hypothesis that manipulation of the electrical stimulation waveform can be used to selectively activate specific neural elements. Specifically, our results are consistent with the prediction that cathode-leading asymmetric waveforms preferentially stimulate cell bodies over axons, while symmetric waveforms preferentially activate axons over cell bodies. The findings here provide some initial steps toward the design and optimization of microstimulation of neural circuitry, and open the door to more sophisticated engineering tools, such as nonlinear system identification techniques, to develop technologies for more effective control of activity in the nervous system.

(Some figures may appear in colour only in the online journal)

1. Introduction

Electrical stimulation of neural tissue has been utilized for more than a century to either probe neural circuitry [1–9] or create desired percepts [10–16] (for a review, see [17, 18]). Following the success of cochlear implant technology, numerous efforts have been carried out to electrically stimulate various sensory cortical regions to provide surrogate sensory signals for applications in visual and somatosensory prostheses [19–22], to restore sensory function and aid in sensorimotor learning for closed-loop brain–computer interfaces and

motor prosthetics [23, 24]. Although recent advancement in technology has enabled cell-type selective activation of neurons through optical stimulation [25], the barriers to clinical implementation for these techniques make electrical microstimulation the most likely route in the near term for clinical means of controlling neural circuitry on relatively fast time scales for sensory prosthetics in humans.

Despite intense investigation of the anatomy and physiology of sensory pathways in the nervous system, beyond the sensory periphery little is known about how to generally and systematically control activity in these pathways.

Although recent work has successfully demonstrated that it is possible for electrical microstimulation to produce simple tactile and visual percepts that contain the same information as those generated by natural sensory stimuli [10, 12], it is currently unclear how to control neural circuitry on a temporal and spatial scale that relates to more complex, naturalistic sensory inputs. In the context of sensory prostheses, given the prevalence and preservation of well-organized topographic maps in all sensory modalities, it is likely that the similarity between neuronal activation patterns evoked by electrical microstimulation and those evoked by natural sensory stimuli plays a key role in minimizing training time and mental load in disabled individuals who use the sensory prostheses. Few studies have systematically compared cortical activation patterns evoked by electrical microstimulation and those evoked by natural sensory stimuli, or investigated how the various parameters of microstimulation may play a role in shaping the spatiotemporal activation of the circuitry (one such study is [26]). The neural responses to electrical stimulation have primarily been studied at the single-cell level [17, 27–29] and the behavioral level [17, 30, 31], with comparatively few studies investigating how electrical stimulation activates a network [32, 33]. In awake behaving animals, electrical stimulation has been shown to deliver enough information to the brain to allow animals to perform equally well in sensory discrimination tasks as compared to their performance with natural sensory stimuli [10, 12]. However, in humans, electrical stimulation has occasionally been described as painful [34, 35], unnatural [34, 35] or discordant [36]. These results are hypothesized to derive from the activation of axons residing close to the electrode tip, but originating from cell bodies far from the electrode, instead of direct stimulation of cell bodies in the immediate vicinity of the electrode. Single-cell electrical stimulation studies lend support to this hypothesis [28, 29].

Definitive support has been supplied by a recent study in which the composite neural activity of an *in vivo* network was recorded in response to direct electrical stimulation of the circuit, indicating that axonal elements near the electrode are activated to produce a sparse and distributed activity within the network [37]. In this study and others, neuronal excitability as a function of electrical microstimulation parameters such as pulse duration, current amplitude, pulse frequency and polarity of the leading phase has been experimentally investigated [17]. However, recent modeling work has suggested that microstimulation waveform shape may play a significant role in the preferential activation of cell bodies versus axons [38], and this hypothesis has not been experimentally validated [39].

Here, we used voltage-sensitive dye (VSD) imaging to quantify *in vivo*, network level spatiotemporal cortical activation in response to electrical microstimulation of the thalamic region that provides direct input to cortex in the rat vibrissa pathway. In general, thalamic microstimulation evoked cortical activation that was both more spatially spread and topographically biased compared to that evoked from natural sensory stimulation. However, utilizing electrical microstimulation with cathode-leading asymmetric waveforms significantly reduced the bias of cortical activation and also increased the spatial specificity of

cortical activation. Systematically increasing the asymmetry of the microstimulation pulses gradually reduced the topographic cortical activation bias. Our data strongly support the hypothesis that electrical pulses with cathode-leading asymmetric waveforms preferentially activate cell bodies over axons, while electrical pulses with either symmetric or anodeleading asymmetric waveforms preferentially activate axons over cell bodies. The findings here provide some initial steps toward the design and optimization of microstimulation of neural circuitry, and open the door to more sophisticated engineering tools, such as nonlinear system identification techniques, to develop technologies for more effective control of activity in the nervous system.

2. Materials and methods

2.1. Surgery and preparation

Fourteen female adult albino rats (220-350 g; Sprague Dawley, Charles River Laboratories, Wilmington, MA) were used in the study. All procedures were approved by the Institutional Animal Care and Use Committee at the Georgia Institute of Technology, and were in agreement with guidelines established by the National Institutes of Health. Briefly, female albino rats were sedated with 2% vaporized isoflurane and anesthetized with sodium pentobarbital (50 mg kg⁻¹, i.p., initial dose); supplemental doses were given as needed to maintain a surgical level of anesthesia, confirmed by measurements of heart rate, respiration and eyelid/pedal reflexes to averse stimuli (toe or tail pinch). In all experiments, body temperature was maintained at 37 °C by a servocontrolled heating blanket (FHC, Bowdoinham, ME). After initial anesthesia, the animal was mounted on a stereotactic device (Kopf Instruments, Tujunga, CA) in preparation for the surgery and subsequent recordings. Atropine (0.5 mg kg⁻¹, s.c.) was injected, and Lidocaine was applied to the tissue on top of the head. After the initial midline incision on the head, tissue and skin were resected, and connective tissue was carefully removed. A craniotomy (\sim 3 mm \times 4 mm) was made on the left hemisphere over the barrel cortex (stereotactic coordinates: 1.0-4.0 mm caudal to the bregma, and 3.5–7.0 mm lateral to the midline) and over the ventroposterior medial nucleus (VPm) of the thalamus (2.0-4.0 mm caudal, 2.0–3.5 mm lateral to the midline [40]). A dam was constructed with dental acrylic around the craniotomy over the barrel cortex to contain the VSD solution (RH1691, 1.5 mg ml⁻¹, Optical Imaging Ltd, Rehovot, Israel) for staining. Mineral oil was periodically applied to the cortical surface over VPm to keep the brain moist. After the recording session, the animal was sacrificed with an overdose of sodium pentobarbital. A subset of the animals were transcardially perfused with 4% paraformaldehyde, and their brains removed for histologically producing the anatomical barrel cortex map.

2.2. VSD imaging

VSD imaging was achieved by using a high-speed, low-noise camera coupled with a tandem lens (MiCAM 2, SciMedia, Tokyo, Japan). After the craniotomy over the barrel cortex, the

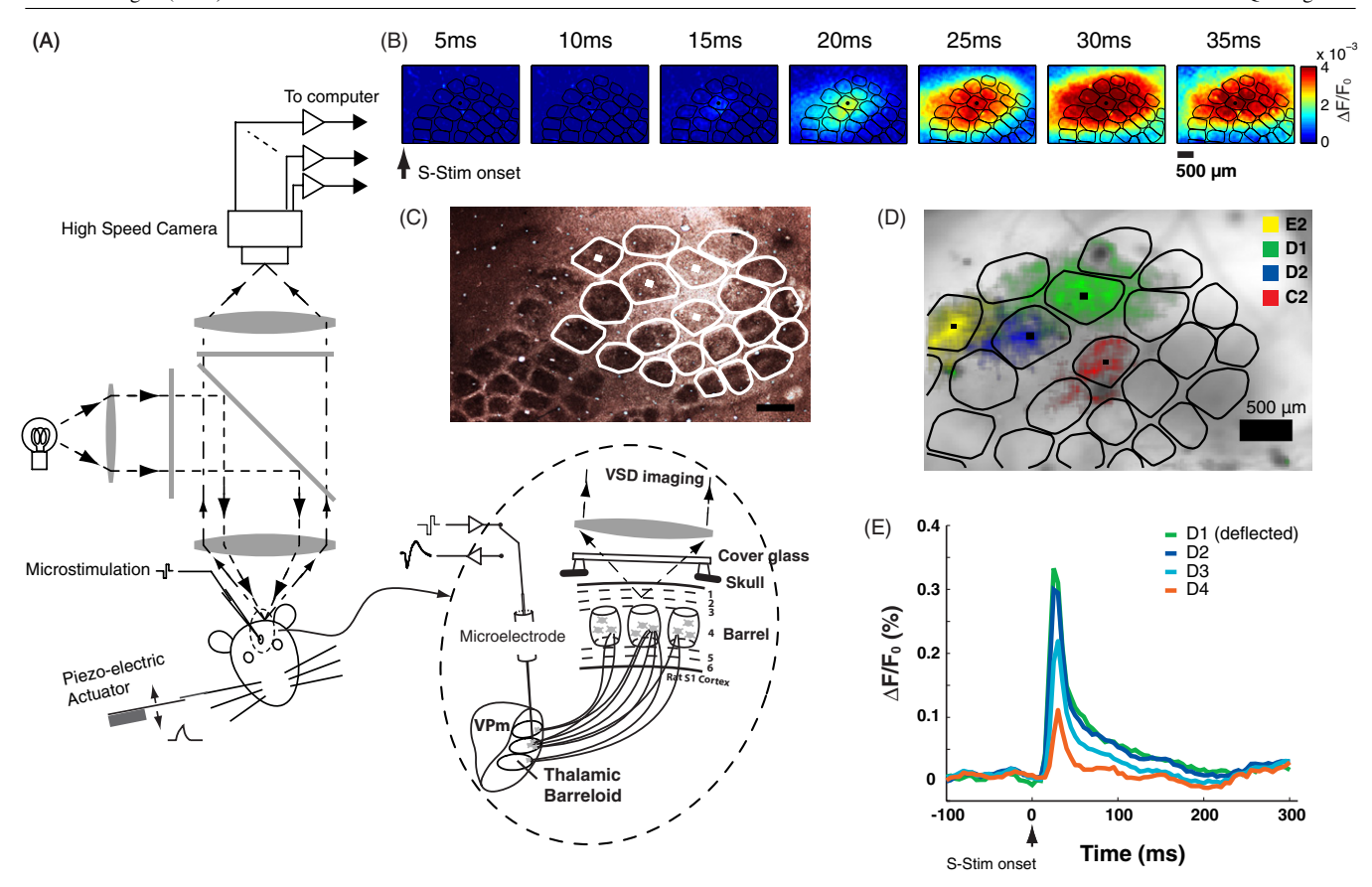


Figure 1. Voltage-sensitive dye imaging of cortical activation in response to thalamic activation and whisker deflection. (A) Diagram of the optical imaging setup. (B) Example of cortical response to a punctate deflection of whisker D2 (sensory stimulation, S-Stim). (C) Example of barrel columns shown in a CO stained brain slice. The white traces are contours of the barrel columns shown in figure 1(D). (D) Barrel mapping by registering the histologically identified barrel map with functional columns. (E) Mean activation within nearby cortical columns D1, D2, D3 and D4 following the punctate deflection of the D1 whisker. Scale bars in B, C and D are 500 μ m.

dura mater was allowed to dry for 15 min [41]. The cortex was stained with the dye RH1691 solution (1.5 mg ml $^{-1}$; Optical Imaging) for 2 h, during which the dye solution was circulated every 5 min to prevent the cerebral spinal fluid from impeding the staining. After staining, saline was applied generously to wash off the dye residue. Then the dam was filled with saline and a glass cover slide was placed on top of the dam to prevent the saline from vaporizing. The dye was excited by a 150 W halogen lamp filtered to pass wavelengths only in the 615–45 nm band. In all experiments, a $1.0 \times$ magnification lens was used as the objective lens in conjunction with a $0.63 \times$ condenser lens to provide $1.6 \times$ magnification, forming a tandem lens as shown in figure 1(A). Twenty trials of VSD data were collected for each stimulus and they were averaged offline for the data analysis (see section 2.8 below).

2.3. Electrophysiological recordings

Extracellular recordings in the VPm were obtained by using single tungsten microelectrodes ($\sim 1~M$, 75 μm in diameter, FHC, Bowdoinham, ME). The detailed procedure was described previously [42]. Briefly, after the craniotomy, a tungsten microelectrode was slowly advanced into VPm using a hydraulic micropositioner (Kopf Instruments, Tujunga, CA). During electrode advancement through VPm, individual

whiskers were stimulated manually to identify the principal whisker (PW), i.e. the whisker that evokes the strongest response. In a subset of experiments, the single-unit responses to the PW and the adjacent whiskers were recorded, a typical example of which is shown in figure 2(B). We aimed at recruiting barrel fields in the E and D rows, which are located close to the center of the imaging field in our preparation. In 14 experiments, the D1 barreloid was accessed six times, the D2 barreloid was accessed once, the D3 barreloid was accessed five times, the E1 barreloid was accessed once and the E3 barreloid was accessed once. Neuronal signals were amplified, band-pass filtered (500–5 kHz), digitized at 30 kHz/channel and collected using a 96-channel data-acquisition system (Blackrock Microsytems, Salt Lake City, UT, USA).

2.4. Thalamic microstimulation

After the PW was identified, the thalamic electrode was used to deliver single electrical current pulses to evoke cortical responses in the somatosensory pathway. The electrical stimuli were created using a digital stimulus generator (model: DS8000, WPI Inc., Sarasota, FL) and delivered using a digital linear stimulus isolator (model: DLS 100, WPI Inc., Sarasota, FL) acting in current source mode. Additionally, a fast switching relay was used to prevent charge accumulation

on the electrode tip. All individual electrical stimuli were charge balanced. Three types of stimulus waveforms were used in this study: (1) a cathode-leading, symmetric biphasic waveform of 200 ms duration per phase (Symm); (2) a cathode-leading, asymmetric biphasic waveform with 1 ms of cathodal duration and 200 ms of anodal duration (ASymC); and (3) an anode-leading, asymmetric biphasic waveform with 1 ms of anodal duration and 200 ms of cathodal duration (ASymA). In the last part of this study, the asymmetry of the cathode-leading asymmetric, i.e. ASymC, waveform was systematically changed to more precisely determine the effect of the asymmetry on the specificity of electrical stimulation. Asymmetry was defined as the ratio of the duration of the first phase to the duration of the second phase minus one, such that the Symm waveform had an asymmetry of zero and the ASymC waveform had an asymmetry of 4. Waveforms were delivered over a range of current amplitudes (30, 35, 40, 45, 50, 60, 70, 80, 90, 100, 120, 150 mA). In each experiment, eight amplitudes were randomly chosen.

2.5. Whisker stimulation

Sensory stimulation (S-Stim) was applied through computer-controlled whisker deflections. Whiskers were trimmed at approximately 12 mm from the face and were inserted into a glass pipette fixed to the end of a calibrated multi-layered piezoelectric bimorph bending actuator (range of motion: 1 mm, bandwidth: 200 Hz; Physik Instrumente (PI), Auburn, MA) positioned 10 mm from the vibrissa pad. Vibrissae were always deflected in the rostral-caudal plane. Punctate deflections consisted of exponential rising and falling phases (99% rise time, 5 ms; 99% fall time, 5 ms) and angular deflection velocities of 75, 150, 225, 300, 450, 600, 900 and 1200 deg s⁻¹ were used as mechanical probe stimuli (S-Stim).

2.6. Histology

Methods were adapted from Wong-Riely (1979) [43], with modifications adapted from Silverman and Tootell (1987) [44]. Briefly, the cortex was flattened to 1 mm and fixed in 4% paraformaldehyde for 12 h. Tangential sections of 70 μm were washed for 10 min in 10% sucrose in 0.1 M phosphate buffer, 10 min in 10% sucrose in 0.05 M Tris with 275 mg L^{-1} cobalt chloride and then three times in PBS before being incubated at 37 °C for 5 h in the staining solution (0.5 g L^{-1} DAB, 50 g L^{-1} sucrose and 75 mg L^{-1} cytochrome c in 0.1 M PB).

2.7. Barrel mapping

The VSD data collected in response to whisker stimulation were functionally registered to the histological map of the barrel cortex [45]. The contours of the barrel cortex columns, shown in figure 1(C), were outlined using the Neurolucida software (MBF Bioscience, Williston, VT) and imported into Matlab. The cortical columns were determined in the VSD data by deflecting a single whisker using a piezoelectric actuator and recording the cortical response. An example of the spatiotemporal VSD response to a single whisker deflection is shown in figure 1(B). The initial frame of cortical activation,

which has previously been shown to be restricted to a single cortical column [46], was captured for individual deflection of four to six different whiskers during each experiment. An example of the VSD response to the deflection of four different whiskers is overlaid in figure 1(D). A least-squares algorithm was used to map the histologically identified anatomical barrel cortex map to the functional barrel cortex map measured through the VSD imaging. The histologically identified barrel map was registered with the functional column mapping from VSD by solving the following linear inverse problem [47]:

$$\begin{bmatrix} u_1 \\ u_2 \\ \vdots \\ v_1 \\ v_1 \\ v_2 \\ \vdots \\ \vdots \\ u_n \end{bmatrix} = \begin{bmatrix} x_1 & y_1 & 1 & 0 \\ x_2 & y_2 & 1 & 0 \\ \vdots & \vdots & 1 & 0 \\ x_n & y_n & 1 & 0 \\ y_1 & -x_1 & 0 & 1 \\ \vdots & \ddots & \ddots & \ddots & \ddots \\ \vdots & \vdots & \ddots & \ddots & \vdots \\ x_n & y_n & 1 & 0 \\ \vdots & \vdots & \ddots & \vdots \\ x_n & y_n & 1 & 0 \\ \vdots & \vdots & \ddots & \vdots \\ x_n & y_n & 1 & 0 \\ \vdots & \vdots & \ddots & \vdots \\ x_n & y_n & 1 & 0 \\ \vdots & \vdots & \ddots & \vdots \\ x_n & y_n & 1 & 0 \\ \vdots & \vdots & \ddots & \vdots \\ x_n & y_n & 1 & 0 \\ \vdots & \vdots & \ddots & \vdots \\ x_n & y_n & 1 & 0 \\ \vdots & \vdots & \ddots & \vdots \\ x_n & y_n & 1 & 0 \\ \vdots & \vdots & \ddots & \vdots \\ x_n & \vdots & \vdots & \vdots \\ x_n & y_n & 1 & 0 \\ \vdots & \vdots & \vdots & \vdots \\ x_n & \vdots & \vdots & \vdots \\$$

where the set of u_i and v_i are the coordinates of the center of mass of VSD activation following each whisker deflection, x_i and y_i are the coordinates of the centroid of each barrel column in the histology frame of reference and A, θ , t_x and t_y represent the scale, rotation and translation, respectively, to register the two coordinate axes.

If histology was not available for a given experimental day, the histological map from other experimental sessions that produced the best fit was used. We have found that histologically identified anatomical barrel cortex maps were consistent across animals in terms of structure, and there was no qualitative difference in the results when histological maps were interchanged across experiments.

2.8. VSD response analysis

All analyses were conducted using Matlab (Mathworks, Natick, MA). VSD responses to mechanical deflection of whiskers (S-Stim) and to thalamic electrical stimulation, i.e. Symm, ASymC and ASymA, were averaged over 20 trials. The averaged responses at each frame were then fitted with 2D Gaussians [48]. The center of the 2D Gaussian was considered as the center of cortical activation. To estimate the area of cortical activation, the frames prior to the stimulus onset were used to estimate the background noise. Only activation greater than three times the level of the background noise was considered. The area of the intersection of the 2D Gaussian and the plane of three times the background noise was defined as the activation area, as shown in figure 3(B). If the magnitude of the 2D Gaussian was less than three times the background noise, the activation area was considered to be zero.

A vectorized method was used to capture both the magnitude and direction of the offset between the VSD center of mass and the center of the barrel electrophysiologically matched to the electrode location (principal barrel). The center of the principal barrel was defined as the origin of the coordinate system. Because the barrel map orientation within the VSD imaging window was not strictly the same for each experimental session, another reference location was needed

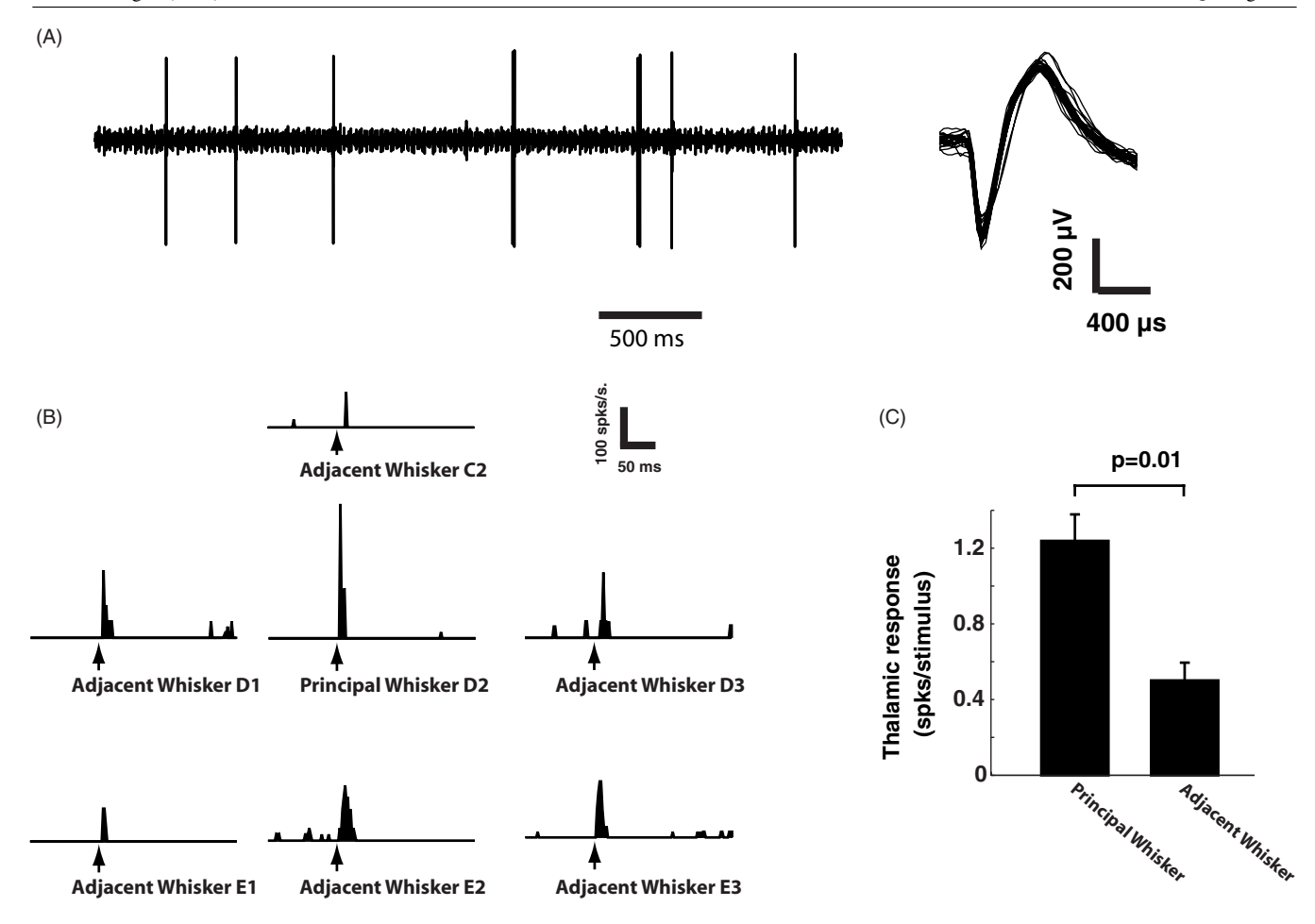


Figure 2. Functional validation of thalamic electrode placement. (A) A typical example of single-unit activity recorded in VPm (left) and spike waveforms (right). (B) The peri-stimulus time histograms (PSTHs) of a VPm cell in response to punctate deflection of whisker C2, D1, D2, D3, E1, E2 and E3 (binsize = 2 ms). (C) Selection of the PW was confirmed by the fact that PW evoked stronger spiking activity than adjacent whiskers (AW) (p = 0.01, Mann–Whitney U-test).

to ensure the consistency of the coordinate system from day to day. The vector $\overrightarrow{r_0}$ (black vectors in figure 4(C)), given by the whisker immediately caudal to the PW, is used to define the zero degree direction. Within this coordinate system, the magnitude and direction of the VSD response relative to the principal barrel are given by the vector $\overrightarrow{r_{VSD}}$ (blue and red vectors in figure 4(C)) connecting the origin to the center of mass of the VSD response. The distance metric used in figures 4 and 5 is given by the average of the magnitude of $\overrightarrow{r_{VSD}}$ across experimental sessions. The topographic bias measurement used in figure 4 is given by the angle between $\overrightarrow{r_{VSD}}$ and $\overrightarrow{r_0}$. The coherence in this bias across experiments is calculated using the vector strength given by the following equation, where θ is the angle from the ith experimental session [49]:

vector strength =
$$\frac{1}{n}$$
 $\cos \theta_i$ $\cos \theta_i$ $\cos \theta_i$ $\cos \theta_i$ $\cos \theta_i$. (2)

3. Results

All measurements were conducted in the thalamocortical circuit of the rodent vibrissa/whisker pathway in vivo. The

basic setup for whisker stimulation, thalamic recording and microstimulation, and imaging of cortical activation is shown in figure 1(A) (see section 2). The spatiotemporal dynamics of whisker-driven cortical responses were measured using VSD imaging in vivo. Deflection of a single mystacial whisker attached to a computer-controlled multilayer piezoelectric actuator (see section 2) evoked a robust cortical response 15– 25 ms following the facial whisker deflection, consistent with previous studies [46]. An example cortical response is shown in figure 1(B), with a sequence of VSD frames following the whisker deflection displaying the fluorescence generated through changes in the membrane voltage. Note that the histologically generated column/barrel map is superimposed for reference (black traces). Each cortical column is primarily associated with one facial whisker, termed the principal whisker. Figure 1(C) shows the histological map of the barrel cortex, and figure 1(D) illustrates the histologically generated columnar map (see section 2) superimposed on the optical image of the brain surface. The initial cortical activations induced by deflection of the E2, D1, D2 and C2 whiskers are color-coded and superimposed here for illustration (note that here we use the classical nomenclature for naming the facial whiskers [50]). Although the cortical activation was initially topographically restricted in and around the column/barrel

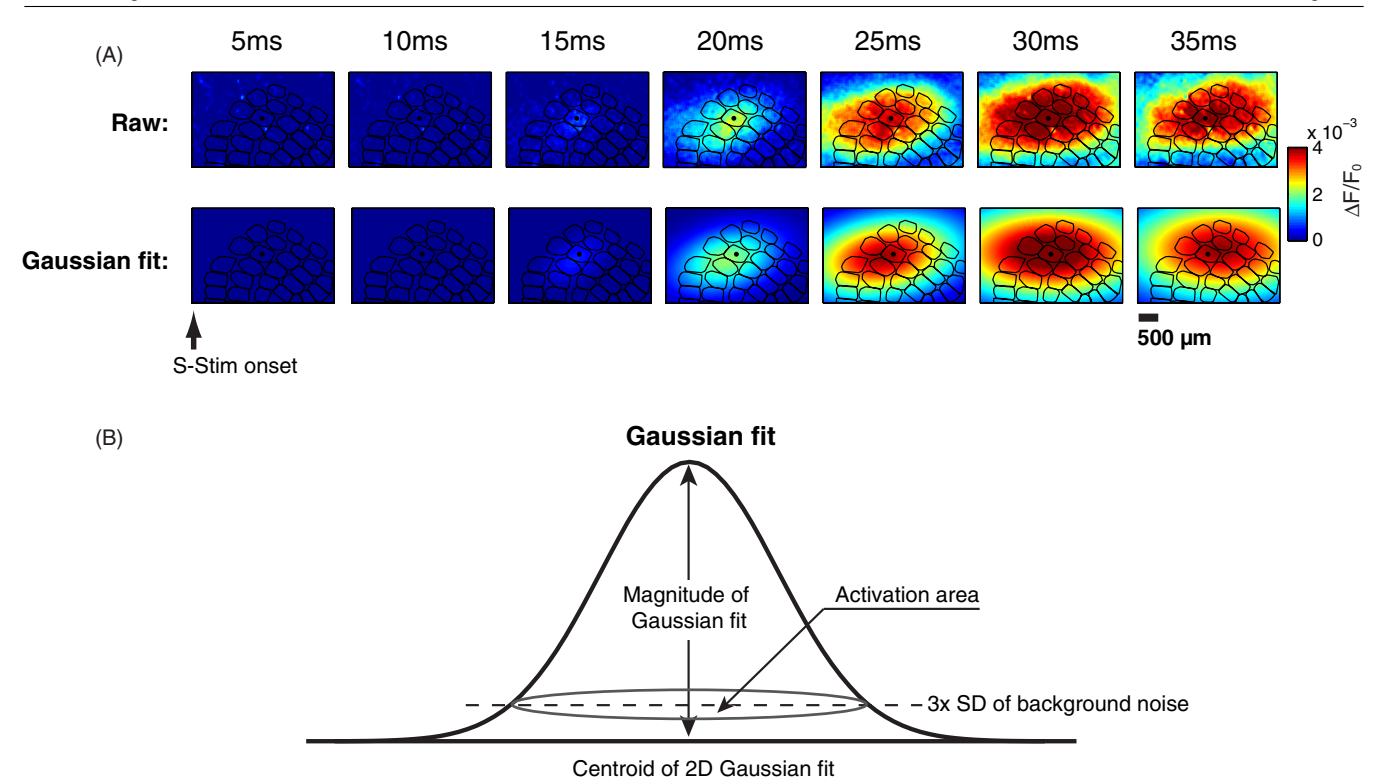


Figure 3. Quantification of the VSD response. (A) Example of a raw VSD image sequence (top) and its 2D Gaussian fit (bottom) following whisker stimulation. (B) Parameters of the 2D Gaussian fit.

associated with the PW, the cortical response quickly spread across a large number of adjacent columns following a single whisker deflection, as seen in figure 1(B). The example in figure 1(E) shows the mean activation within several nearby cortical columns (D1, D2, D3 and D4) following the deflection of the D1 whisker, illustrating the time course of the spatial spread of cortical activation.

Functional validation of thalamic electrode placement. A critical analysis here is that of the comparison of the cortical response to stimulation of a single whisker (sensory stimulation, or S-Stim) with that induced by thalamic microstimulation (electrical stimulation, or E-Stim). It is thus necessary to precisely map the position of the stimulating electrode within the thalamic VPm relative to the whisker array on the face. This was achieved by recording whisker-driven spiking activity in response to a punctate deflection applied to individual whiskers in the array. The PW was defined as that whisker which evoked the strongest spiking activity in terms of the mean spike count within a 30 ms window following the whisker deflection [42]. Figure 2(A) shows typical single-unit activity recorded in VPm, with a trace of the raw signal (left) and overlaid spike waveforms (right). Figure 2(B) shows the peri-stimulus time histograms (PSTHs) for the VPm recording in response to a single punctate stimulus (see section 2) of different whiskers (E1, E2, E3, D1, D2, D3, C2), where the D2 whisker evoked the largest response in this particular case, and was therefore the primary whisker for this electrode placement. On average, the PW elicited significantly more

spikes per deflection compared to the adjacent whiskers (AWs) (p = 0.01, Mann–Whitney U-test, n = 7, figure 2(C)), consistent with previous studies [51].

Q Wang et al

Quantification of the VSD response. To quantify the cortical activation evoked by whisker deflection and thalamic microstimulation, the VSD images were each fitted with a two-dimensional Gaussian function (see section 2). A typical VSD sequence following whisker stimulation is shown in figure 3(A). The raw sequence is shown in the top row, and the corresponding colormap of the Gaussian fit is shown in the bottom row. Note that despite the topographic relationship between the facial whisker and a particular cortical column (as outlined in black, where the primary column/barrel is denoted with a black dot), following the activation onset at 20 ms post-stimulus, there was a significant spread of the activation across a large region of the cortical barrel map, consistent with previous findings [46]. To quantify the nature of the cortical response, the magnitude of the cortical response was defined as the magnitude of the Gaussian fit, and the area of the cortical activation was defined as the region of intersection of the Gaussian fit with a plane positioned at three times the standard deviation of the pre-stimulus VSD signal (i.e. noise), as illustrated in figure 3(B).

Thalamic microstimulation results in a systematic topographical bias in cortical activation. The locus of activation of the primary somatosensory cortex carries important information about the somatotopy of the

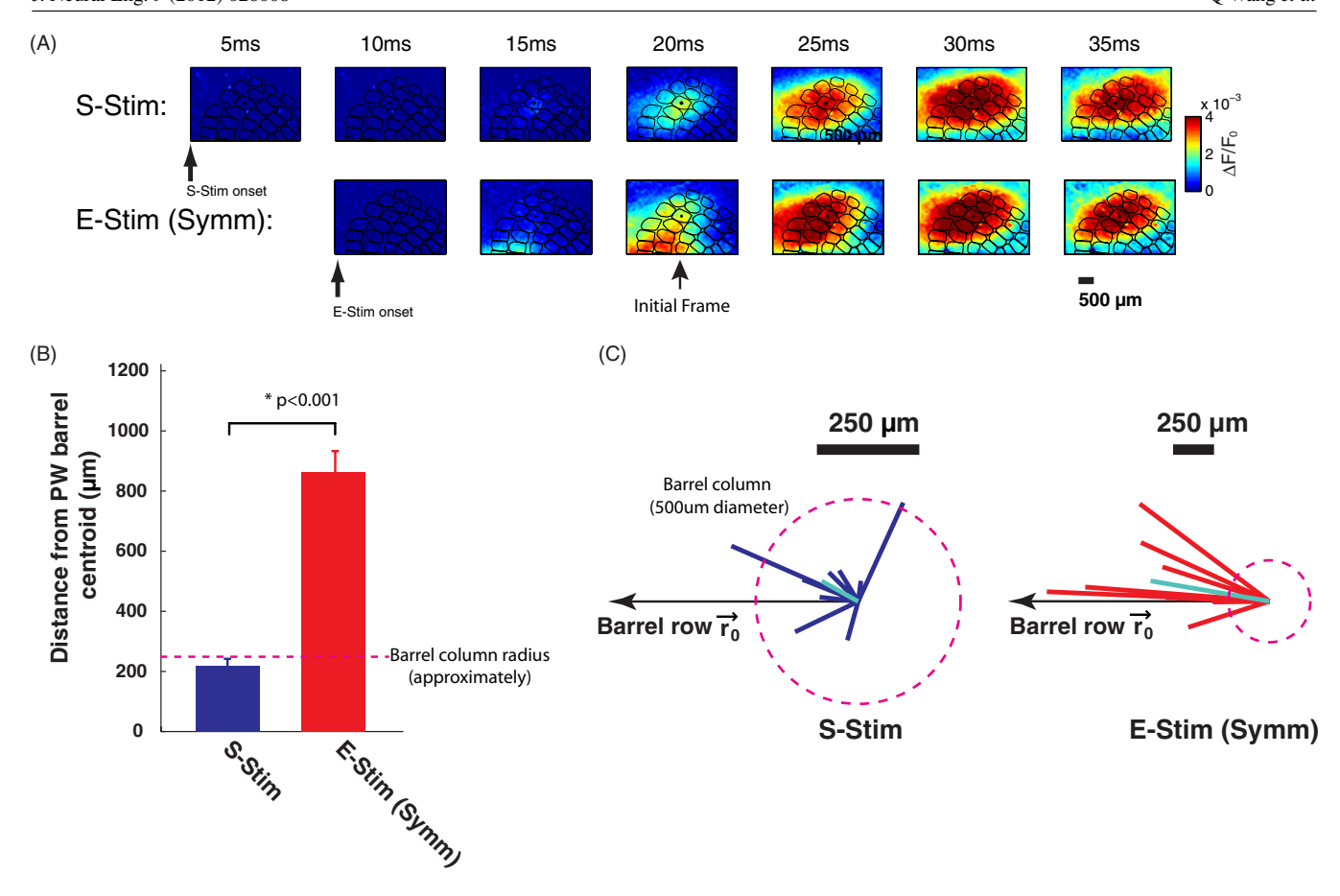


Figure 4. Thalamic microstimulation with symmetric waveforms results in a systematic topographical bias in cortical activation. (A) Top: typical VSD response to whisker stimulation. Bottom: typical VSD response to thalamic microstimulation with a symmetric waveform. (B) The centroid of the VSD signal in response to thalamic microstimulation (Symm) diverged significantly more from the center of the actual cortical column than the centroid of the VSD signal in response to sensory stimulation (S-Stim). (C) The distribution of vectors computed as the difference between the centroid of cortical activation and the actual center of the cortical column/barrel for both S-Stim and E-Stim (Symm) (p < 0.001, Wilcoxon signed-rank test, n = 9). The vectors from the E-stim (Symm) response show a consistent topographical bias.

body surface. Activation of cortex through thalamic microstimulation revealed a systematic bias in the locus of activation that was not seen for the sensory stimulus. Figure 4(A) shows a typical VSD response, where the top row is the sequence of VSD images taken following a punctate deflection of a single whisker (S-Stim), and the bottom row is the sequence of VSD images taken after a single microstimulation pulse was delivered to the corresponding topographically aligned region in the VPm thalamus (E-Stim). The E-Stim was a conventional symmetric biphasic current pulse waveform (60 μ A in amplitude, 200 μ s per phase). It is qualitatively apparent from this example that the locus of cortical activation was different between the S-Stim and E-Stim cases, and that the initial onset of activation from E-Stim was not topographically aligned with the cortical column/barrel to which this region of VPm thalamus projects (denoted with black dot in the center of the overlaid columnar map) as it is for the S-Stim response (top row).

The centroid of the Gaussian fit of the VSD signal was then used to quantify this effect, specifically through the distance between the centroid measured from the VSD signal (at onset frame) and the actual center of the column. On average, the centroid of cortical activation in response to the sensory stimulus was within the cortical column/barrel (distance less than 250 μ m, which is approximately the radius of a cortical column/barrel, denoted by the dashed line in figure 4(B)). In contrast, the centroid of the Gaussian fit of the VSD signal in response to thalamic microstimulation diverged significantly from the center of the actual cortical column (distance of centroid to actual center >850 μ m, figure 4(B)). The misalignment of the cortical activation with the actual barrel/column corresponding to the whisker/electrode location was significantly greater for the thalamic microstimulation than for the whisker stimulation (p < 0.001, Wilcoxon signed-rank test, figure 4(B), n = 9). Furthermore, we have found that there was no correlation between topographic bias and stimulus intensity (p = 0.539, Mann–Whitney U test).

The discrepancy between the centroid of cortical activation in response to thalamic microstimulation and the centroid of the principal barrel column might be due to increased variability in the measurement of the centroid of the VSD in the case of the thalamic microstimulation. In this scenario, we would expect the centroid of the cortical activation to be randomly located relative to the actual center

of the barrel/column. Figure 4(C) shows the distribution of vectors computed as the difference between the centroid of cortical activation and the actual center of the cortical column/barrel, capturing both the magnitude and direction. While the vectors measuring discrepancy for the S-Stim case exhibited a more dispersed distribution and an overall difference well within the actual column (left plot, the light blue line shows average, relative to the column denoted by the dashed circle), the vectors associated with the thalamic microstimulation exhibited a strong bias along the cortical columns associated with a row of whiskers (right plot). To quantify this notion, we used the vector strength to measure how well the vectors were aligned along a common direction, as opposed to randomly dispersed [49] (see section 2). Indeed, the vectors in the thalamic microstimulation case were more locked to the direction along the barrel row (vector strength: 0.91, figure 4(C): right) than in the whisker deflection case (vector strength: 0.63, figure 4(C): left), pointing to a systematic bias in the cortical activation in response to thalamic microstimulation.

Cathode-leading asymmetric microstimulation significantly improved the topographic activation of cortex. Modeling studies have suggested that the conventional symmetric, charge-balanced current waveform pulse (utilized in figure 4) may preferentially activate axons as opposed to cell bodies [38]. In contrast, it has been asserted that using biphasic current pulses with asymmetric waveforms can preferentially activate cell bodies. If the bias in cortical activation exhibited in figure 4 is due to the activation of fibers of passage rather than cell bodies local to the electrode tip, then an asymmetric pulse design may alleviate some of this problem. Using a cathode-leading asymmetric waveform for the thalamic microstimulation significantly decreased the discrepancy between the centroids of cortical activation and the actual center of the barrel/column. This is first shown qualitatively in figure 5(A), where the top row is again the sequence of VSD images following whisker stimulation, the middle row following thalamic microstimulation with a symmetric current injection waveform and the third row following thalamic microstimulation with an asymmetric, cathode-leading current injection waveform. Qualitatively, we see that the asymmetric microstimulation results in an initial onset of cortical activation that is more topographically aligned with the response to the whisker stimulation, as compared to the symmetric microstimulation. The quantification in figure 4(B) was repeated for the asymmetric, cathodeleading case, and resulted in a significant decrease in the topographic discrepancy (from >850 μ m to 617 μ m, p = 0.003, Wilcoxon signed-rank test, figure 5(B), n =9). Therefore, cathode-leading asymmetric microstimulation significantly diminished the discrepancy between the centroids of cortical activation and the centroid of the principal barrel, improving the topographic activation of cortex. To rule out the possibility that this improvement was due to the difference of the derivative of charge delivered (the total charge per phase was the same for both AsymC and Symm, and the amplitudes of the anodal phase were the same), we also tested the anode-leading asymmetric waveform, which is the flip of the cathode-leading asymmetric waveform. In contrast to the cathode-leading asymmetric waveform, the cortical activation induced by the anodeleading asymmetric waveform diverged even further from the correct topographic location than that for the symmetric microstimulation waveform (p < 0.001, Wilcoxon signed-rank test, figure 5(B), n = 9). Interestingly, the difference in the topographic localization of the cortical responses induced by the different microstimulation waveforms was most prominent at the onset of cortical activation (initial frame), and was reduced as the VSD signal propagated beyond the initial frame (figure 5(C)).

The topographic alignment of the cortical activation was enhanced with increasing asymmetry of the microstimulation waveform. To measure the effects of temporal asymmetry in the charge delivery of the microstimulation on the localization of the cortical response, the degree of asymmetry in the microstimulation pulse was systematically varied. Specifically, a measure of asymmetry was defined as the duration of the cathodal phase over the duration of the anodal phase minus one, where the perfectly symmetric waveform has an asymmetry measure of zero, and increasing the duration of the initial cathodal component of the waveform increases the measure of asymmetry, as shown in figure 6(A). Note that the waveform in each case was charge balanced, yielding a net charge delivery of zero over the duration of the waveform. The discrepancy between the centroid of cortical activation and the center of the actual column/barrel exponentially decayed with the asymmetry of the waveform, and saturated at approximately 650 μ m (figure 6(B)).

Cathode-leading asymmetric waveform also improved the specificity of thalamic microstimulation. In addition to affecting the locus of activation following thalamic microstimulation, the waveform properties also had a significant effect on the magnitude and area of cortical activation following microstimulation. As shown in figure 3(B), the magnitude of the cortical response was defined as the magnitude of the two-dimensional Gaussian fitted to the cortical VSD signal, and the area of cortical activation was defined as the size of the cortical region spanned by the two-dimensional Gaussian at a magnitude of three times the standard deviation of the background noise. In general, the area and magnitude of the cortical activation increased with increasing stimulus strength. Figure 7(A) shows the relationship between increasing angular velocity of the punctate whisker deflection and the magnitude (left) and area (middle) of cortical activation, with a monotonic increase in each. The area of activation was coupled to the magnitude, with a fairly linear relationship (figure 7(A), right). Similarly, with the thalamic microstimulation, there was an increase in the magnitude and area of cortical activation with increasing amplitude of the current pulse, shown for the symmetric and asymmetric cases in the left and middle panels of figure 7(B) and (C). Again, in both of these cases, the magnitude and area of cortical activation were coupled, exhibiting a fairly linear relationship for each (figures 7(B) and (C), right panels). In

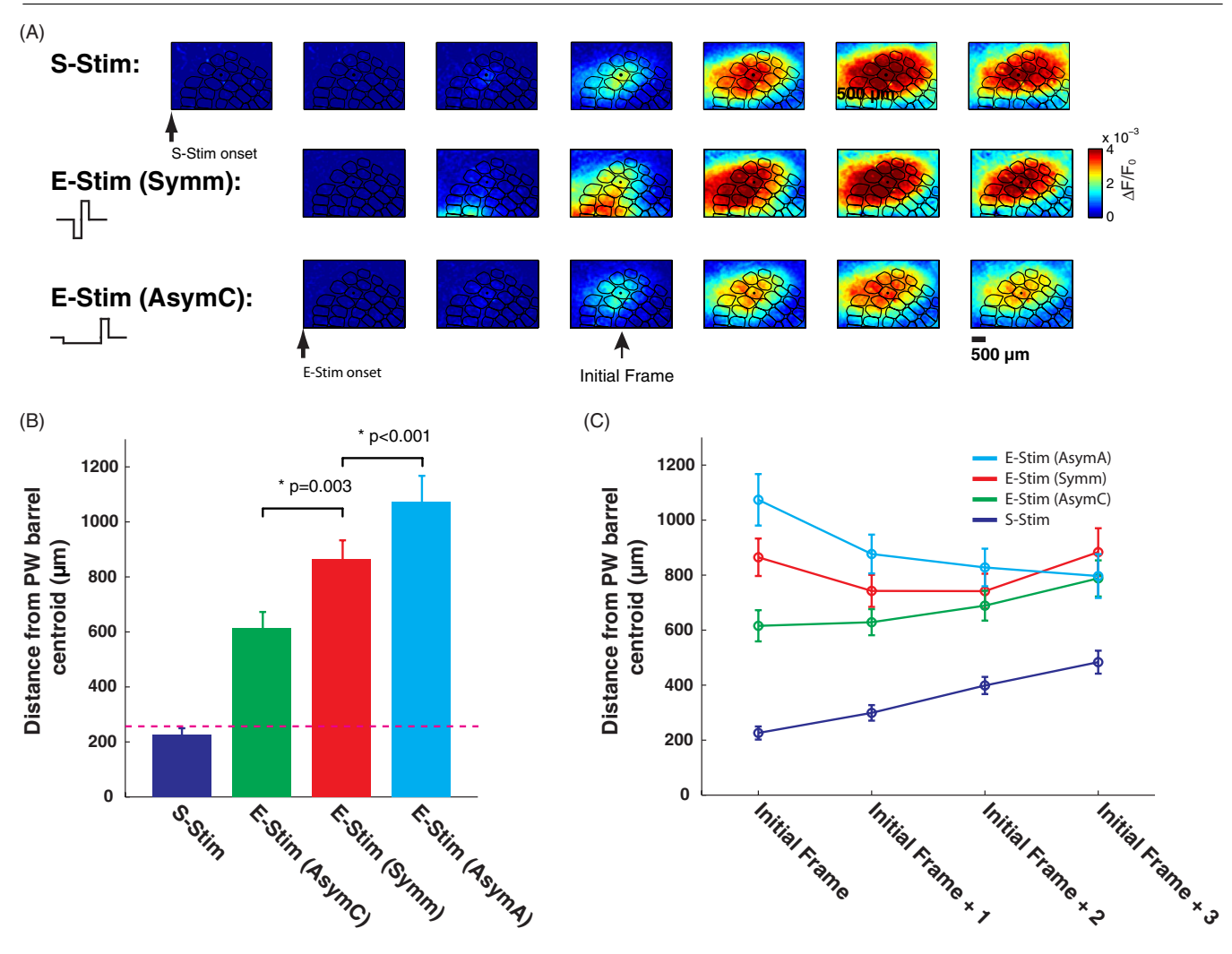


Figure 5. Cathode-leading asymmetric microstimulation significantly improved the topographic activation of cortex. (A) Top: typical VSD response to whisker stimulation. Middle: typical VSD response to thalamic microstimulation with a symmetric waveform (Symm). Bottom: typical VSD response to thalamic microstimulation with a cathode-leading asymmetric waveform (AsymC). The examples shown here are from the same experimental session. (B) Topographic discrepancy of VSD signals in response to S-Stim, E-Stim (AsymC), E-Stim (Symm) and E-Stim (AsymA). Cathode-leading asymmetric microstimulation significantly decreased the topographic discrepancy (p = 0.003, Wilcoxon signed-rank test, n = 9). In contrast, anode-leading asymmetric microstimulation significantly enlarged the topographic discrepancy (p < 0.001, Wilcoxon signed-rank test, n = 9). (C) The difference in the topographic localization of the cortical responses induced by the different microstimulation waveforms was most prominent at the onset of cortical activation (initial frame) and was reduced as the VSD signal propagated beyond the initial frame.

utilizing the thalamic microstimulation as a surrogate input to the pathway, the nominal goal is to activate the cortex in a manner that is consistent with that of sensory stimulation (S-Stim, figure 7(A)). To activate the appropriate area of cortex associated with a particular angular velocity of the tactile input, for example, the current amplitude of the microstimulation pulse can be adjusted. However, for the symmetric waveform, the cortical response was quite widespread, resulting in an area of activation that would be substantially greater than that corresponding to the sensory stimulation, even for relatively low values of current near threshold. Furthermore, the coupling of the area and magnitude of activation was such that if the magnitude of activation were matched to that of the sensory stimulation, the area of activation would be too large, and if the area of activation were matched to that of the sensory

stimulation, the magnitude would be too low. This was not the case for the asymmetric microstimulation waveform. This is well captured by comparing the slopes of the relationships between the area and magnitude of activation for each case, as shown in figure 7(D), where the slope for the symmetric case was significantly lower than that for sensory stimulation, but using an asymmetric waveform resulted in a slope much closer to that of the sensory stimulation.

4. Discussion

Here we characterized the response of the primary somatosensory cortex to both peripheral tactile stimulation and electrical stimulation of the thalamic region providing direct input to the barrel cortex. Conventional symmetric

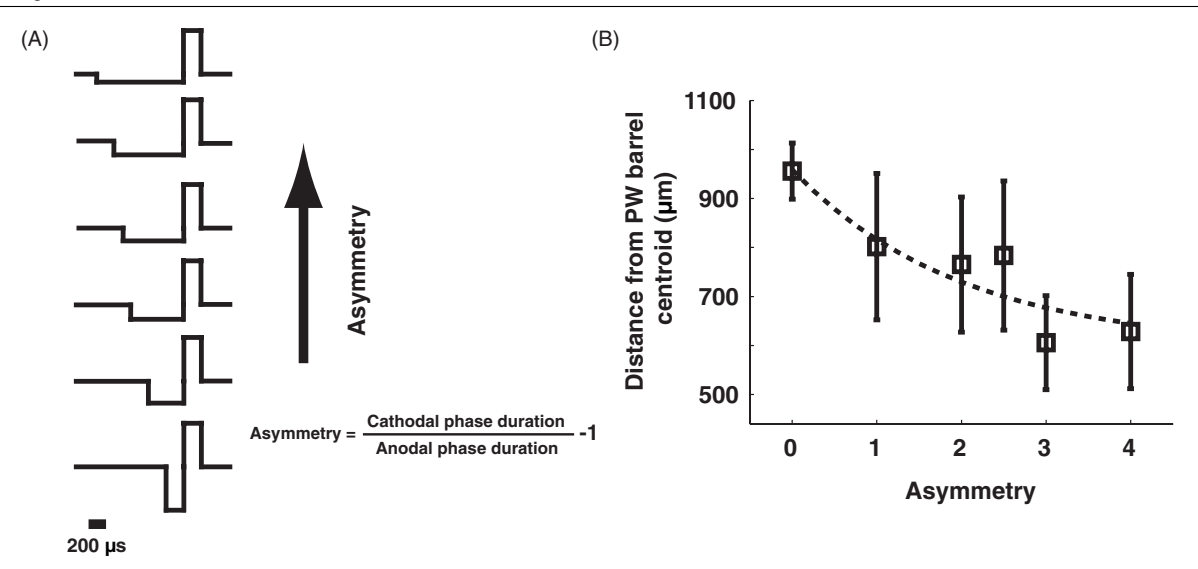


Figure 6. The topographic alignment of the cortical activation was enhanced with increasing asymmetry of the microstimulation waveform. (A) Asymmetric waveforms with different asymmetry. Asymmetry was defined as the duration of the cathodal phase over the duration of the anodal phase minus one, where the perfectly symmetric waveform has an asymmetry measure of zero. (B) The topographic discrepancy exponentially decayed with the asymmetry of the waveform and saturated at approximately 650 μ m.

biphasic electrical stimulation activated a broad region of the cortex centered at a region that was multiple cortical columns away from the cortical column which was topographically aligned with the electrode location. Although not directly assessed here, the consequences of this topographic mismatch would likely produce undesired percepts because previous work with brain imaging has suggested that there is a strong correlation between cortical activation and perception [52, 53]. Previous studies using thalamic stimulation in humans have reported that percepts induced by electrical stimulation are often unnatural or discordant with relation to the anatomical electrode position [34–36], potentially linked to the phenomena we describe here.

Although it has been hypothesized that the aberrant sensations resulting from microstimulation are due to the activation of axons passing by the electrode tip in addition to the nearby cell bodies, the downstream neural response causing these sensations has not been studied in detail for functional validation. Beyond the sensory periphery, the anatomy of the circuitry places neuronal cell bodies and axonal fiber tracts within close proximity of one another. As a result, microstimulation can activate neurons with cell bodies that are quite far from the site of stimulation [37, 54], beyond that predicted by conventional understanding of how electric fields grow with the magnitude of the current injection. What has been observed is that neurons with cell bodies very distal to the stimulation site can still be activated for very small currents, attributed to the crossing of fiber tracts through the volume of tissue affected by the electric field, resulting in what Butovas and Schwarz refer to as a spatiotemporal 'blurring' of the activation. In a more recent study, two-photon microsocopy was utilized to observe the neural responses to nearby electrical stimulation in vivo. Through this technique, the authors provide strong evidence that electrical stimulation principally activates axons within a very short radial distance from the electrode [37].

Previous modeling work predicts that alterations in the stimulation waveform change the relative stimulation thresholds for cell bodies near the electrode and passing axons [38]. This is hypothesized to occur through differential inactivation of sodium channels at the cell body and nearest node of Ranvier caused by the long subthreshold cathodal phase of the asymmetric stimulus waveform [38, 55]. The sodium channels at the node of Ranvier are inactivated by the depolarizing cathodal pulse and then the subsequent short duration, high current anodal phase preferentially stimulates the nearby cell bodies. Although this study does not provide observation at this level of detail, functionally we observed a distinct difference in cortical response when using symmetric versus asymmetric stimulation that is consistent with this notion. Whereas the response to symmetric stimulation was centered multiple cortical columns away from the cortical column topographically matched to the electrode position, the response to asymmetric stimulation was shifted more closely to the anatomically expected cortical column. Additionally, recent work in awake behaving rats has shown that cathode-leading asymmetric waveforms had higher detection thresholds than symmetric waveforms for intracortical microstimulation [56]. This finding is consistent with our results and together they suggest that asymmetric and symmetric stimulation likely activate different neural elements. Further investigation is necessary to more directly determine whether asymmetric pulses provide increased selectivity of cell bodies over axons.

Although the exact anatomy of the projecting fibers from the VPm thalamus to layer 4 of the primary somatosensory cortex has not been fully understood, histological evidence suggests that fibers from VPm regions (barreloids) associated with more rostral tactile input pass by the VPm barreloids associated with more caudal input on the way to the primary somatosensory cortex [57, 58]. Given this anatomical

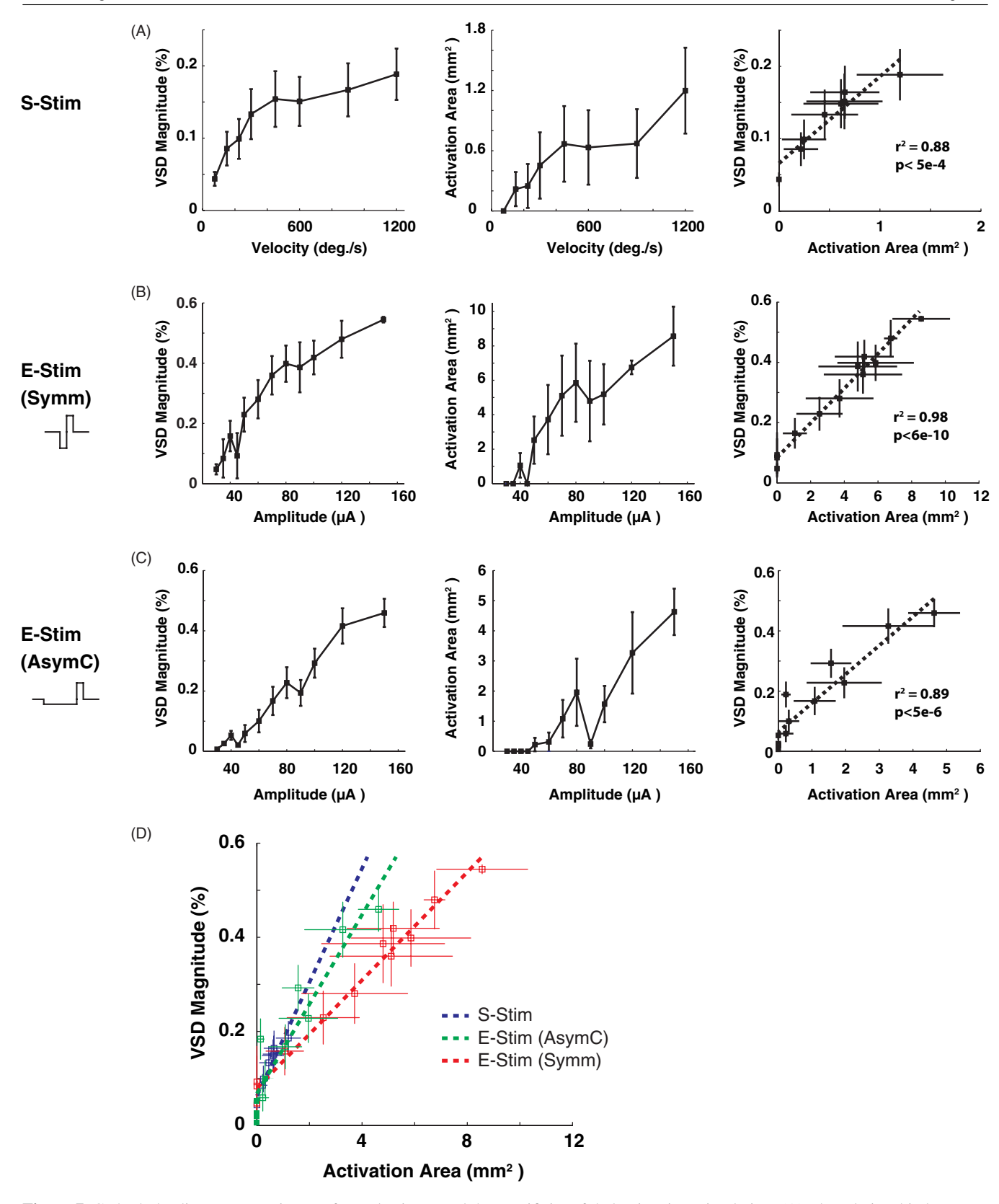


Figure 7. Cathode-leading asymmetric waveform also improved the specificity of thalamic microstimulation. (A) The relationship between the increasing angular velocity of the punctate whisker deflection and the magnitude (left) and area (middle) of cortical activation. Right: the approximately linear relationship between the area of activation and the magnitude. (B) The relationship between the increasing amplitude of the current pulse with symmetric waveform and the magnitude (left) and area (middle) of cortical activation. Right: the approximately linear relationship between the area of activation and the magnitude. (C) The same as in (B) for E-Stim (AsymC). (D) The slopes of the relationships between the area and magnitude of activation for S-Stim, E-Stim (AsymC) and E-Stim (Symm). Using the asymmetric waveform resulted in a slope much closer to that of the sensory stimulation (S-Stim).

arrangement, we would expect that if symmetric stimulation preferentially activates axons as opposed to cell bodies, the cortical activation would be centered in the cortical columns corresponding to whiskers more rostral than the whisker corresponding to the electrode location. Indeed, we observed a systematic topographic bias in the center of mass of the cortical response toward cortical columns representing rostral inputs when using symmetric stimulation. The systematic topographic bias, in concert with previous histological evidence, strengthens the support for the hypothesis that asymmetric stimulation increases the selectivity stimulation of cell bodies versus axons.

While the results presented here are specific to stimulation of the VPm region of the somatosensory thalamus in the rodent, we expect the phenomenon to be consistent in other regions of the brain, and thus the findings here are general. We use thalamic stimulation due to the extensive literature detailing the anatomical and functional characterization of the thalamocortical circuit in the rodent vibrissa system [59–61], and the fact that it provides direct, mono-synaptic input to cortical layer 4 in the vibrissa region. Furthermore, stimulation in the thalamus paired with recording in the cortex allows us to observe the direct neural response to electrical stimulation on a network level by recording only two synapses downstream of the stimulation, with VSD imaging of layer 2/3 cortical activity. Importantly, the site of the stimulating electrode in the VPm thalamus is approximately 4 mm from the site of the VSD imaging in the cortex, implying that the observed cortical activation is due to engagement of the thalamocortical circuit, rather than passive conduction through the tissue. The VSD imaging proves ideal for this study due to its high spatial and temporal resolution, allowing a full characterization of the spatiotemporal cortical response to a point source of current in the thalamus [41, 62]. While the VSD signal is limited to layer 2/3 activity due to light scattering, it has been shown that early periods of activation in layer 2/3 reflect the activation patterns within layer 4, suggesting that the VSD imaging at the activation onset is likely very similar to the activity of the input layer 4 [46]. It should be noted that the topographic misalignment of the cortical activity in response to thalamic microstimulation is most pronounced at the onset of cortical activation. However, the later stage of activation spreads across a large region of cortex and even so, some degree of disrupted somatotopy does persist following the initial activation. The coding of any sensory stimuli more complex than the unitary impulses we utilize here could thus not rely on later stages of cortical activation to alleviate the problem. Initial activation of areas not topographically aligned with the desired percept would preclude subsequent or concurrent activation of that region in the context of more rich, spatiotemporal sensory stimuli. Finally, although the VSD activity has been linked to sub-threshold membrane potentials, and thus the measured signals do not directly reflect action potentials, action potentials do obviously accompany strong depolarizations and the hard-thresholding we apply to the VSD imaging likely captures the distinction.

Our findings have strong implications for delivering information to the brain for sensory prosthetics applications.

Microstimulation disrupts the somatotopy that the brain strives to maintain throughout development, possibly through the activation of passing axon fiber tracts, which would be a problem in almost all brain regions including the most simply arranged anatomy of the periphery. This could lead to nearby electrodes producing similar or overlapping perceptions if the same axons pass by each electrode. For instance, Grill et al reported that humans, in response to thalamic microstimulation, often experience parathesias that are localized to a different somatotopic region than the mapped sensory receptive field of the stimulating electrode, a phenomenon termed 'discordant parethesia' [36]. While it is clear that the capabilities for plasticity and learning in the brain improve the likelihood of success in interpreting this surrogate signaling to the brain, there is a fundamental limit in that the sensations must be discriminable to be functionally useful [63]. This problem could be alleviated by ensuring that a oneto-one topographic map is preserved, even if different from that of the normal physiology. By more closely adhering to the normal somatotopy, asymmetric stimulation pulses ensure that sensations produced by nearby electrodes are less affected by the underlying axonal anatomy and more likely to be distinct and natural sensations. Additionally, asymmetric stimulation pulses result in cortical responses that have a higher spatial specificity, and much closer to normal sensory stimulation, than symmetric biphasic pulses. Given that the discriminability of information delivered to the brain is likely affected by the overlap of the cortical responses to neighboring inputs, asymmetric cathodal stimulation would thus likely increase the functional resolution of a sensory prosthetic.

Given that this study was focused on electrical microstimulation, it is unclear how these findings might impact newly developed techniques for optical activation of neural tissue. Just as injection of even very small (\sim 10 μ A) currents into the cortex can activate thousands of neurons proximal to the electrode tip [64], optical stimulation at typical experimentally applied power ranges may activate tissue in a region on the order of a cubic millimeter [65]. Furthermore, the axonal tracts of neurons expressing optogenetic proteins contain a high enough concentration of the light-activated channels to generate action potentials via optical stimulation [66], potentially leading to the same issues faced with electrical microstimulation. However, unlike electrical microstimulation, optogenetic-based techniques may provide the much-needed selectivity that will permit differential activation of sub-populations of neurons that are not segregated spatially. Through genetic expression or viral transfection, different cell types can be targeted to express specific channels that can be optically activated to depolarize or hyperpolarize the cell [67]. If this type of selectivity can be extended to differentially activate cell bodies and axons, the issue of somatotopic misalignment we describe here may be further resolved.

Taken together, the results here provide some initial directions in the design of charge delivery for topographically activating downstream circuits through electrical microstimulation. Future experimental and modeling studies may further optimize the stimulus design and expand

the problem to more complex patterns of microstimulation across electrode arrays, which are requisite to deliver the high amount of information embedded in the sensory environment. Just as this study sought to characterize and control the nonlinearities involved in the spatial activation profile of a single stimulus pulse, future work must also address the dynamic nonlinearity that governs the neural response to temporal sequences of stimulation in order to gain precise control of complex neural circuits, which is essential for high fidelity sensory prosthetic technology.

Acknowledgments

This work was supported by the National Institutes of Health (NIH Grant R01NS48285). The authors would like to thank Clare Gollnick for the assistance in histology.

References

- [1] Fritsch E and Hitzig G 1870 Uber die elektrische erregbarkeit des grosshims *Arch. Anat. Physiol. wiss. Med.* **37** 300–32
- [2] Salzman C D, Britten K H and Newsome W T 1990 Cortical microstimulation influences perceptual judgements of motion direction *Nature* 346 174–7
- [3] Swadlow H A and Lukatela K 1996 Cross-correlation and microstimulation: complementary tools in the extracellular analysis of synaptic interactions *J. Neurosci. Methods* 64 219–25
- [4] Graziano M S A, Taylor C S R and Moore T 2002 Complex movements evoked by microstimulation of precentral cortex Neuron 34 841–51
- [5] Moore T and Armstrong K M 2003 Selective gating of visual signals by microstimulation of frontal cortex *Nature* 421 370–3
- [6] Tolias A S, Sultan F, Augath M, Oeltermann A, Tehovnik E J, Schiller P H and Logothetis N K 2005 Mapping cortical activity elicited with electrical microstimulation using fMRI in the macaque Neuron 48 901–11
- [7] Butovas S, Hormuzdi S G, Monyer H and Schwarz C 2006 Effects of electrically coupled inhibitory networks on local neuronal responses to intracortical microstimulation *J. Neurophysiol.* 96 1227–36
- [8] Yang Y, DeWeese M R, Otazu G H and Zador A M 2008 Millisecond-scale differences in neural activity in auditory cortex can drive decisions *Nature Neurosci.* 11 1262–3
- [9] Gaunt R A, Hokanson J A and Weber D J 2009 Microstimulation of primary afferent neurons in the L7 dorsal root ganglia using multielectrode arrays in anesthetized cats: thresholds and recruitment properties J. Neural Eng. 6 055009
- [10] Romo R, Hernandez A, Zainos A and Salinas E 1998 Somatosensory discrimination based on cortical microstimulation *Nature* 392 387–90
- [11] Humayun M S et al 2003 Visual perception in a blind subject with a chronic microelectronic retinal prosthesis Vis. Res.
 43 2573–81
- [12] Pezaris J S and Reid R C 2007 Demonstration of artificial visual percepts generated through thalamic microstimulation *Proc. Natl Acad. Sci.* 104 7670–5
- [13] Butovas S and Schwarz C 2007 Detection psychophysics of intracortical microstimulation in rat primary somatosensory cortex Eur. J. Neurosci. 25 2161–9
- [14] Houweling A R and Brecht M 2008 Behavioural report of single neuron stimulation in somatosensory cortex *Nature* 451 65–8

- [15] Parker R A, Davis T S, House P A, Normann R A and Greger B 2011 The functional consequences of chronic, physiologically effective intracortical microstimulation Brain Machine Interfaces: Implications for Science, Clinical Practice and Society (Progress in Brain Research vol 194) ed M G J Schouenborg and N Danielsen (Amsterdam: Elsevier) chapter 11 pp 145–65
- [16] Venkatraman S and Carmena J M 2011 Active sensing of target location encoded by cortical microstimulation *IEEE Trans. Neural Syst. Rehabil. Eng.* 19 317–24
- [17] Tehovnik E J, Tolias A S, Sultan F, Slocum W M and Logothetis N K 2006 Direct and indirect activation of cortical neurons by electrical microstimulation J. Neurophysiol. 96 512–21
- [18] Clark K L, Armstrong K M and Moore T 2011 Probing neural circuitry and function with electrical microstimulation *Proc.* R. Soc. B 278 1121–30
- [19] Normann R A, Greger B A, House P, Romero S F, Pelayo F and Fernandez E 2009 Toward the development of a cortically based visual neuroprosthesis *J. Neural Eng.* 6 035001
- [20] Bradley D C et al 2005 Visuotopic mapping through a multichannel stimulating implant in primate v1 J. Neurophysiol. 93 1659–70
- [21] Tehovnik E J, Slocum W M, Smirnakis S M and Tolias A S 2009 Microstimulation of visual cortex to restore vision *Prog. Brain Res.* 175 347–75
- [22] Pezaris J S and Eskandar E N 2009 Getting signals into the brain: visual prosthetics through thalamic microstimulation Neurosurg. Focus 27 E6
- [23] O'Doherty J E, Lebedev M, Hanson T L, Fitzsimmons N and Nicolelis M A L 2009 A brain–machine interface instructed by direct intracortical microstimulation Front. Integr. Neurosci. 3 20
- [24] Rebesco J M and Miller L E 2011 Enhanced detection threshold for in vivo cortical stimulation produced by Hebbian conditioning J. Neural Eng. 8 016011
- [25] Boyden E S, Zhang F, Bamberg E, Nagel G and Deisseroth K 2005 Millisecond-timescale, genetically targeted optical control of neural activity *Nature Neurosci.* 8 1263–8
- [26] Weber D J, London B M, Hokanson J A, Ayers C A, Gaunt R A, Torres R R, Zaaimi B and Miller L E 2011 Limb-state information encoded by peripheral and central somatosensory neurons: implications for an afferent interface *IEEE Trans. Neural Syst. Rehabil. Eng.* 19 501–13
- [27] Stoney S D, Thompson W D and Asanuma H 1968 Excitation of pyramidal tract cells by intracortical microstimulation: effective extent of stimulating current *J. Neurophysiol.* 31 659–69
- [28] Nowak L G and Bullier J 1998 Axons, but not cell bodies, are activated by electrical stimulation in cortical gray matter: i. Evidence from chronaxie measurements *Exp. Brain Res*. 118 477–88
- [29] Nowak L G and Bullier J 1998 Axons, but not cell bodies, are activated by electrical stimulation in cortical gray matter: ii. Evidence from selective inactivation of cell bodies and axon initial segments Exp. Brain Res. 118 489–500
- [30] Murasugi C M, Salzman C D and Newsome W T 1993 Microstimulation in visual area MT: effects of varying pulse amplitude and frequency J. Neurosci. 13 1719–29
- [31] Tehovnik E J, Slocum W M, Carvey C E and Schiller P H 2005 Phosphene induction and the generation of saccadic eye movements by striate cortex J. Neurophysiol. 93 1–19
- [32] Civillico E F and Contreras D 2005 Comparison of responses to electrical stimulation and whisker deflection using two different voltage-sensitive dyes in mouse barrel cortex in vivo J. Membr. Biol. 208 171–82

- [33] Logothetis N K, Augath M, Murayama Y, Rauch A, Sultan F, Goense J, Oeltermann A and Merkle H 2010 The effects of electrical microstimulation on cortical signal propagation *Nature Neurosci.* 13 1283–91
- [34] Ohara S, Weiss N and Lenz F A 2004 Microstimulation in the region of the human thalamic principal somatic sensory nucleus evokes sensations like those of mechanical stimulation and movement *J. Neurophysiol.* **91** 736–45
- [35] Patel S, Ohara S, Dougherty P M, Gracely R H and Lenz F A 2006 Psychophysical elements of place and modality specificity in the thalamic somatic sensory nucleus (ventral caudal, vc) of awake humans J. Neurophysiol. 95 646–59
- [36] Grill W M, Simmons A M, Cooper S E, Miocinovic S, Montgomery E B, Baker K B and Rezai A R 2005 Temporal excitation properties of paresthesias evoked by thalamic microstimulation Clin. Neurophysiol. 116 1227–34
- [37] Histed M H, Bonin V and Reid R C 2009 Direct activation of sparse, distributed populations of cortical neurons by electrical microstimulation *Neuron* 63 508–22
- [38] McIntyre C C and Grill W M 2000 Selective microstimulation of central nervous system neurons Ann. Biomed. Eng. 28 219–33
- [39] Grill W M, Norman S E and Bellamkonda R V 2009 Implanted neural interfaces: biochallenges and engineered solutions Annu. Rev. Biomed. Eng. 11 1–24
- [40] Paxinos G and Watson C 1998 The Rat Brain in Stereotaxic Coordinates (New York: Academic)
- [41] Lippert M T, Takagaki K, Weifeng X, Huang X and Jian-Young W 2007 Methods for voltage-sensitive dye imaging of rat cortical activity with high signal-to-noise ratio J. Neurophysiol. 98 502–12
- [42] Wang Q, Webber R and Stanley G B 2010 Thalamic synchrony and the adaptive gating of information flow to cortex *Nature Neurosci.* 13 1534–41
- [43] Wong-Riley M 1979 Changes in the visual system of monocularly sutured or enucleated cats demonstrable with cytochrome oxidase histochemistry *Brain Res.* 171 11–28
- [44] Silverman M S and Tootell R B H 1987 Modified technique for cytochrome oxidase histochemistry: increased staining intensity and compatibility with 2-deoxyglucose autoradiography *J. Neurosci. Methods* 19 1–10
- [45] Wallace D J and Sakmann B 2008 Plasticity of representational maps in somatosensory cortex observed by *in vivo* voltage-sensitive dye imaging *Cerebral Cortex* 18 1361–73
- [46] Petersen C C H, Grinvald A and Sakmann B 2003
 Spatiotemporal dynamics of sensory responses in layer 2/3
 of rat barrel cortex measured *in vivo* by voltage-sensitive
 dye imaging combined with whole-cell voltage recordings
 and neuron reconstructions *J. Neurosci.* 23 1298–309
- [47] Millard D C, Wang Q and Stanley G B 2011 Nonlinear system identification of the thalamocortical circuit in response to thalamic microstimulation 5th Int. IEEE/EMBS Conf. on Neural Engineering (NER) pp 1–4
- [48] Chen Y, Geisler W S and Seidemann E 2006 Optimal decoding of correlated neural population responses in the primate visual cortex *Nature Neurosci.* 9 1412–20
- [49] Goldberg J M and Brown P B 1969 Response of binaural neurons of dog superior olivary complex to dichotic tonal stimuli: some physiological mechanisms of sound localization *J. Neurophysiol.* **32** 613–36

- [50] Diamond M E, M von Heimendahl, Knutsen P M, Kleinfeld D and Ahissar E 2008 'Where' and 'what' in the whisker sensorimotor system *Nature Rev. Neurosci.* 9 601–12
- [51] Bruno R M, Khatri V, Land P W and Simons D J 2003 Thalamocortical angular tuning domains within individual barrels of rat somatosensory cortex J. Neurosci. 23 9565–74
- [52] Chen L M, Friedman R M and Roe A W 2003 Optical imaging of a tactile illusion in area 3b of the primary somatosensory cortex Science 302 881–5
- [53] Benoit M M, Raij T, Lin F-H, Jakelinen I P and Stufflebeam S 2010 Primary and multisensory cortical activity is correlated with audiovisual percepts *Human Brain Mapp.* 31 526–38
- [54] Butovas S and Schwarz C 2003 Spatiotemporal effects of microstimulation in rat neocortex: a parametric study using multielectrode recordings *J. Neurophysiol.* 90 3024–39
- [55] Grill W M and Mortimer J T 1997 Inversion of the current– distance relationship by transient depolarization *IEEE Trans. Biomed. Eng.* 44 1–9
- [56] Koivuniemi A S and Otto K J 2011 Asymmetric versus symmetric pulses for cortical microstimulation *IEEE Trans. Neural Syst. Rehabil. Eng.* 19 468–76
- [57] Haidarliu S and Ahissar E 2001 Size gradients of barreloids in the rat thalamus J. Comparative Neurol. 429 372–87
- [58] Wimmer V C, Bruno R M, de Kock C P J, Kuner T and Sakmann B 2010 Dimensions of a projection column and architecture of VPM and POm axons in rat vibrissal cortex Cerebral Cortex 20 2265–76
- [59] Simons D J and Carvell G E 1989 Thalamocortical response transformation in the rat vibrissa/barrel system J. Neurophysiol. 61 311–30
- [60] Sherman S M and Guillery R W 1996 Functional organization of thalamocortical relays J. Neurophysiol. 76 1367–95
- [61] Miller K D, Pinto D J and Simons D J 2001 Processing in layer 4 of the neocortical circuit: new insights from visual and somatosensory cortex Curr. Opin. Neurobiol. 11 488–97
- [62] Grinvald A and Hildesheim R 2004 VSDI: a new era in functional imaging of cortical dynamics *Nature Rev. Neurosci.* 5 874–85
- [63] Wall J T and Kaas J H 1986 Long-term cortical consequences of reinnervation errors after nerve regeneration in monkeys *Brain Res.* 372 400–4
- [64] Tehovnik E J 1996 Electrical stimulation of neural tissue to evoke behavioral responses J. Neurosci. Methods 65 1–17
- [65] Bernstein J G, Han X, Henninger M A, Ko E Y, Qian X, Franzesi G T, McConnell J P, Stern P, Desimone R and Boyden E S 2008 Prosthetic systems for therapeutic optical activation and silencing of genetically-targeted neurons *Proc. Society of Photo-Optical Instrumentation* Engineers (San Jose, CA) p 6854
- [66] Cruikshank S J, Urabe H, Nurmikko A V and Connors B W 2010 Pathway-specific feedforward circuits between thalamus and neocortex revealed by selective optical stimulation of axons *Neuron* 65 230–45
- [67] LaLumiere R T 2011 A new technique for controlling the brain: optogenetics and its potential for use in research and the clinic *Brain Stimulation* 4 1–6